Препринти Інституту фізики конденсованих систем НАН України розповсюджуються серед наукових та інформаційних установ. Вони також доступні по електронній комп'ютерній мережі на WWW-сервері інституту за адресою http://www.icmp.lviv.ua/

The preprints of the Institute for Condensed Matter Physics of the National Academy of Sciences of Ukraine are distributed to scientific and informational institutions. They also are available by computer network from Institute's WWW server (http://www.icmp.lviv.ua/)

Ярослав Миколайович Ільницький
Стефан Соколовскі
Тарас Миколайович Пацаган

Фазові переходи за посередництва розчинника у порах із стінками декорованими полімерними щітками. Комп'ютерне моделювання методом дисипативної динаміки

Роботу отримано 7 грудня 2012 р.

Затверджено до друку Вченою радою ІФКС НАН України

Рекомендовано до друку відділом комп'ютерного моделювання багаточастинкових систем

Виготовлено при ІФКС НАН України

Національна академія наук України

ІНСТИТУТ ФІЗИКИ КОНДЕНСОВАНИХ СИСТЕМ

ICMP–12–13E

J.M.Ilnytskyi, S.Sokołowski*, T.Patsahan

DISSIPATIVE PARTICLE DYNAMICS STUDY OF SOLVENT MEDIATED TRANSITIONS IN PORES DECORATED WITH TETHERED POLYMER BRUSHES IN THE FORM OF STRIPES

*Department for the Modelling of Physico-Chemical Processes, Maria Curie-Skłodowska University, 20031 Lublin, Poland

ЛЬВІВ

УДК: 538.9

PACS: 62.23.St, 36.20.Ey, 61.20.Ja

Дисипативна динаміка морфологічних перетворень спричинених розчинником у порах із декорованими стінками

Я.М.Ільницький, С.Соколовскі, Т.Пацаган

Анотація. Досліджено формування морфологій у порі, яка має стінки, декоровані смугами полімерних щіток (із мономерів сорту A), та заповнена бінарною сумішшю сортів A і B різної композиції. Знайдено граничні випадки квазі-одновимірного та квазі-двовимірного розшарування сортів. Показано, що формування морфологій та – в деяких випадках – перемикання між ними при зміні композиції суміші спричинене зміною локального середовища для ланцюжків полімерних щіток. Знайдено сформовані за посередництвом розчинника ламеларні, меандро-подібні та рядкові циліндричні фази, для кожної з яких проаналізовано інтеграли перекриття між щітками та компоненти тензора гірації ланцюжків у щітках.

Dissipative particle dynamics study of solvent mediated transitions in pores decorated with tethered polymer brushes in the form of stripes

J.M.Ilnytskyi, S.Sokołowski, T.Patsahan

Abstract. We study self-assembly of a binary mixture of components A and B confined in a slit-like pore with the walls modified by the stripes of tethered brushes of beads A. We concentrate on solvent mediated transitions between morphologies when the composition of the mixture varies. For certain limiting cases of the pore geometry we found an effective reduction of the dimensionality to quasi one- and two-dimensional demixing cases. The change of a local environment for the chains upon varying the mixture composition provides an explanation for formation of a range of morphologies and, in some cases, for switching between them. We found solvent mediated lamellar, meander and in-lined cylinder phases which are analysed quantitatively on the values of brush overlap integrals and the components of a gyration tensor.

Подається в Condensed Matter Physics
Submitted to Condensed Matter Physics

1. Introduction

In recent years investigations of polymer films on solid surfaces have become one of the most rapidly growing research area in physics, chemistry, and material science. The reason for such sustained growth is due to the availability of a wealth of fundamentally interesting information in thermodynamics and kinetics, such as long and short range forces, interfacial interactions, flow, and instability phenomena. [1–6, 8] Moreover, polymer thin films are widely used as an industrial commodity in coatings and lubricants and they have become an integral part of the development process in modern hi-tech applications such as optoelectronics, biotechnology, nanolithography, novel sensors and actuators. [9–16] Most of these applications have been connected with an intrinsic property of polymer films to exhibit a variety of surface morphologies, the size of which ranges from a few tens of nanometers to hundreds of micrometers. As many of the modern, technologically relevant phenomena occur at the nanoscale, the behavior of polymer thin films deposited on flat surface that exhibit morphologies at the nanoscale has been one of major focuses in recent years. [6, 8, 17–22]

The development of several new techniques [23] in material science permits now the productions of solid substrates whose surface is "decorated" with precisely characterized surface structures on length scales ranging from nanometers to microns. In particular, advances in nanotechnology have permitted establishment of methods for obtaining functional polymeric films on solid surfaces exhibiting quite complex topographic nanostructures. Such chemically decorated substrates allow for manipulation of fluid at very short length scales and thus they can play an important role in a variety of contexts. [24–26]

Importance of systems involving brushes tethered at structured surfaces stimulated development of methods of theoretical description of such systems. Theoretical studies of fluids in contact with brushes on patterned surfaces have been mainly based on different simulation methods. They include Monte Carlo [27] and molecular dynamics, [28] as well as dissipative particle dynamics (DPD) simulations. [17, 29] The studies performed so far indicated that heterogeneity of tethered layers has a great impact on the structure of the confined fluid and thermodynamic and dynamic properties of the systems.

In numerous previous studies [29], including our work [30], the simulations have been carried out assuming constant composition in the confined system. However, the demixing phenomena and the formation of different morphologies strongly depend on the composition [32] and

the aim of this work is to get an insight how the change in the fluid composition influences the structure of the confined system. Similarly as in previous work, [30] we use DPD to investigate the behavior of a binary mixture, composed of beads A and B, confined in slit-like pores with walls modified by the stripes of tethered chains that are made of beads A. The stripes at the opposing pore walls are placed "in-phase" (face-to-face), or "out-of-phase. Species A and B are assumed to exhibit demixing in a bulk phase. The simulations are carried out for different compositions of the fluid. Our interest is to determine possible morphologies that can be formed inside the pore, depending on the fluid composition, and on the geometrical parameters characterizing the system (the size of the pore and the width of the stripes, the arrangement of the stripes). In particular, we analyze special limiting cases, where geometry of the pore leads to the reduction of effective dimensionality. Special emphasize is given to the cases of stripes the separation distance between which, either within the pore wall or across the pore, is small. The crossover for the polymer chains from the regime of polymer melt to the regime of a good solution provides a basis for solvent mediated morphology formation and morphology switching. We performed complementary simulations where the solvent in a form of a binary mixture is replaced by one-component solvent of variable quality. Moreover, we also consider how the arrangement of the stripes ("in-" versus "out-of-phase") influences the observed phenomena. Quantitative analysis of morphologies is performed by means of overlap integrals of polymer chains belonging to different stripes or surfaces. Conformational properties of chains are studied via gyration tensor components. The simulation method has been described in our previous work [30] and for the sake of brevity it has been omitted here.

The paper is organized as follows. In the next section we will recall briefly the model and the simulation method. A number of limiting cases for the pore geometry that show the effects of reduced effective dimensionality are considered in section 3. Quantitative analysis of solvent mediated morphologies for the case of weakly separated stripes is performed in section 4. The summary of the results is presented in section 5.

2. The model

To simulate the pore we use the box of the dimensions L_x, L_y and L_z. All the dimensions are in reduced units, measured in respect to the cutoff distance r_c for the repulsive interaction, which is set to $r_c = 1$. The planes $z = 0$ and $z = L_z \equiv d$ are impenetrable walls. Periodic

boundary conditions are applied in both X and Y directions. Each wall is divided into stripes of equal width, w, alternating those with and without polymers attached. The stripes at the apposite walls can be places either in- or out of phase, see Fig. 1. The width of the stripes with attached polymers is the same as the width of the polymer free spaces, therefore the term "out-of-phase" means that the stripe with polymer on one wall is facing polymer free stripe at another wall. The rest of the pore interior is filled by single beads, representing the fluid components.

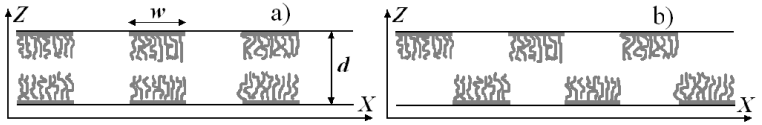

Figure 1. Geometry of the pore with in-phase (a) and out-of-phase (b) arrangement of the stripes with tethered polymer chains. The pore size is d and the stripes width is w. The length of polymer chains is $L = 20$ beads.

In simulations we use DPD approach that includes the existence of smooth repulsive walls with the use of the reflection algorithm that preserves the total momentum. [30] The reduced number density for beads is equal to $\rho = 3.0$. Polymer chains are built of $L = 20$ beads linked via harmonic bonds. The grafting points have been fixed on each wall and distributed randomly inside the stripes with reduced grafting density $\rho_g = 1.0$. More details are provided elsewhere. [30]

Two bead sorts, A and B are considered. Polymer chains are made of beads of sort A. The total number of polymer beads in the system is N_A^p. A binary fluid mixture (which fills the interior of the pore) contains N_A^s beads of sort A and N_B beads of sort B. The fraction of the beads of sort B is $f_B = N_B/N$, where $N = N_A^p + N_A^s + N_B$ is the total number of the beads. Miscibility of A and B beads is adjusted via the value of a_{AB} for the A-B repulsive interaction as compared to the values of a_{AA} and a_{BB} for the A-A and B-B interactions, respectively. [31] In our study we use the following values: $a_{AA} = a_{BB} = 25$ and $a_{AB} = 40$.

For visualization of morphologies we employ the following density grid approach. Simulation box is split into the grid of cubic cells with linear dimension of $0.75-2.0$, depending on the simulation box size. Local densities for polymer A beads, $\rho_A^p(x, y, z)$, solvent A beads, $\rho_A^s(x, y, z)$, and solvent B beads, $\rho_B(x, y, z)$, are evaluated in each cell, centered at (x, y, z). They are averaged over $10 - 15$ configurations (the subsequent configurations are separated by 5000 simulation steps). The averaging

is carried out after stabilization of a given morphology (typically, after $2 \cdot 10^5$ simulation steps).

We found that presenting both local densities of A and B beads in the same snapshot is not very informative. Instead, we show separate snapshots for local density of A or of B beads. In the first case, we represent the cells with low local density of A beads $(\rho_A^p(x,y,z)+\rho_A^s(x,y,z))/\rho < 0.15$ as dots. All other cells are space-filled with the color saturation proportional to the value of $(\rho_A^p(x,y,z)+\rho_A^s(x,y,z))/\rho$. The color tint is blueish if $\rho_A^p(x,y,z) > \rho_A^s(x,y,z)$ and greenish otherwise. Similar approach is used in the second case, when the density of B beads is plotted. In this case $\rho_B(x,y,z)$ is color coded with red tint.

3. Solvent-mediated transitions in special geometries

3.1. Wide stripes geometry

In the case of wide stripes that are in-phase arranged, the periodic pattern of alternating sub-regions is formed within the pore. The sub-regions free of polymer brush provide an environment for a bulk, quasi-3D demixing of confined A and B beads. On the contrary, the sub-regions dominated by a brush, reduce the volume accesible for the demixing of A and B beads to quasi-2D slabs, especially for moderate values of pore size d. This is demonstrated in Fig. 2, where we show examples of morphologies observed for wide stripes with $w = 90$ in a pore of size of $d = 20$ when the fraction f_B is varied.

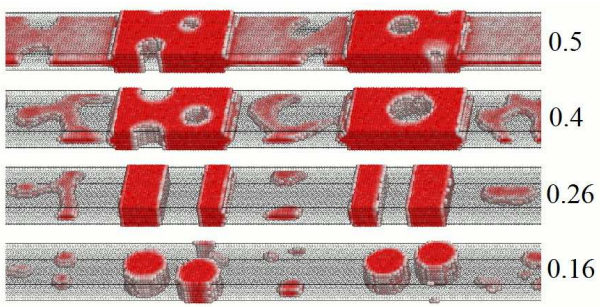

Figure 2. The sequence of morphologies obtained for the case of wide stripes, $w = 90$, at pore size $d = 20$ by varying fraction of B beads, f_B (indicated at the right). Color-coded density of B beads in the selected part of the pore is shown only for the sake of clarity.

The first effect to mention is that with the increase of the fraction of A beads, $f_A = 1 - f_B$, more of them are adsorbed by the stripes of polymer brush causing their considerable swelling. We will discuss this effect quantitatively in section 4. The remaining A and B beads are spread within the rest of accessible volume.

We will concentrate here on the phenomena that occur within quasi-3D sub-regions. The morphologies formed here repeat those observed for diblock copolymers at various composition (or in similar systems). [30,32] To relate both cases one should look at the local fractions of A and B beads here, f'_A and f'_B, that differ from their global counterparts, f_A and f_B due to adsorption of some of A beads into the brush mentioned above. We found that cylinders made of B beads are formed at $f_B = 0.16$ ($f'_B = 0.31$, lowest frame in Fig. 2). Similarly, cylinders made of A beads are observed inside the interval from $f_B = 0.40$ ($f'_A = 0.26$) to $f_B = 0.50$ ($f'_A = 0.17$). Lamellar-like phase (in the OYZ plane; alternating blocks of A and B beads along the X-axis) is observed in the interval from $f_B = 0.26$ ($f'_A = 0.50$) to $f_B = 0.30$ ($f'_A = 0.42$). These boundaries of morphologies (in terms of the values f'_U for minor fraction U) correlate well with the phase diagram for diblock copolymers (see, e.g. Refs. [30, 32])

Morphology transformations observed within quasi-2D regions literally repeat those found for the narrow stripes geometry, and this case is considered in detail in the following subsection.

3.2. Narrow stripes geometry

For narrow stripes, $w < 5$, the polymer chains from adjacent stripes brigde theirselves into lamellae that envelope each wall. [30] It is quite obvious that the same scenario holds for the out-of-phase arrangement of stripes, as far as both surfaces are decoupled. This is confirmed in our simulations (not shown for the sake of brevity). Two flat lamellae, formed at each wall, reduce the region accessible to free A and B beads to a slab, which turns into a quasi-2D one for moderate pore size $d \sim 14-20$. This situation also represents the sub-regions dominated by a brush for the case of wide stripes (considered in a previous subsection).

In Fig. 3 we display the sequence of quasi-2D morphologies that appear in this central slab as the result of a micro-phase separation between A and B beads. The pore size is $d = 13.333$, the stripes width is $w = 4$ and only color-coded density of B beads is shown (in red tint). This pore size is a special one, as far as for the parameters being used here (polymer length, bulk and grafting densities), no solvent A beads are present at $f_B = 0.5$. [30] At this fraction f_B, solvent B beads fill-in all slab-like

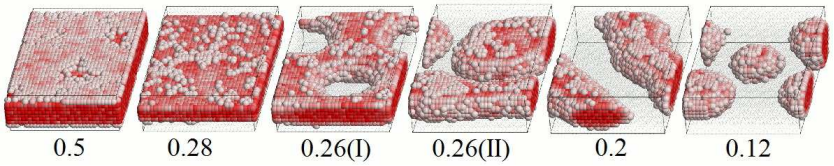

Figure 3. Sequence of morphologies obtained for narrow stripes, $w = 4$, in a pore of size $d = 13.333$ at various fractions f_B (indicated at the bottom). From left to right: lamellar, thinned lamellar, perforated lamellar, "sausage" and "cake", single "sausage", and hexagonally packed "cakes" morphologies are shown (only color-coded density of B beads is shown).

accessible volume in the middle of the pore (first frame from the left in Fig. 3). The slab stays continuous but thinnes out with a decrease of f_B down to $f_B = 0.28$ (the next frame). Then, it turns into a perforated lamellar one and then into disjointed prolate and/or oblate objects made of beads B (see respective frames in Fig. 3). For still lower value of f_B, $f_B \approx 0.12$ hexagonally distributed "cookies" of B beads appear. One can easily see that this morphology possesses the same symmetry as perforated lamellar one, if beads A and B are interchanged. Further decrease of f_B causes that hexagonal order of the "cookies" is lost, and for $f_B < 0.1$ "cookies" of B beads become randomly arranged (not shown). This sequence of the morphologies is reminiscent of the one observed in partial mixing of the two-dimensional fluids. [33] Therefore, the case of narrow stripes can be classified as geometry-driven dimensional crossover from 3D to 2D for confined fluid.

3.3. Pillar geometry

In the case of wider stripes ($w > 6$), bridging of polymer chains that belong to adjacent stripes is prohibited due to high penalty in conformational entropy. Instead, the in-phase arranged stripes can bridge theirselves across the pore to form pillars, providing that the pore width d is not too big (cf. the sketch phase diagram presented in the previous work [30]). Such pillars are observed, for example, at $d = 13.333$ and $w = 10$. Similarly to the case shown in Fig. 2, the system again displays (periodic along X axis) pattern of sub-regions, one being pillars of merged brushes and another – polymer-free sub-regions. At $f_B = 0.5$ the latter are in a form of blocks filled exclusively with solvent B beads. For $0.5 > f_B > 0.26$ these blocks become thinner first (as far as solvent

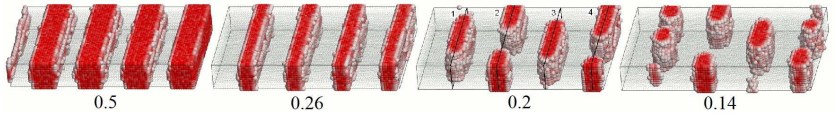

Figure 4. Sequence of morphologies obtained for $d = 13.333$ and $w = 10$ at various fractions f_B (indicated at the bottom). Blocks of B beads filling the space between pillars of A beads ($f_B = 0.50$), thinned blocks ($f_B = 0.26$), hexagonally arranged columns ($f_B = 0.20$), and random columns ($f_B = 0.14$) are shown. Only color-coded density of B beads is displayed.

A beads are adsorbed into pillars causing the latter to swell). Then, for $f_B \sim 0.20$, the blocks split into rounded "columns" spanning across the pore and arranged almost hexagonally. At still lower values of f_B we arrive at randomly arranged columns of B beads of random thickness. All these morphologies are displayed in Fig. 4.

The regions accessible for the micro-phase separation of solvent beads have a shape of slabs extended along Y-axis. The important point here is that all morphologies observed within these slabs at various f_B are uniform within the X dimension of each slab, thus the behavior of the system can be interpreted as being quasi-1D along Y axis within each slab. One can quantify observed morphology changes by the density profiles of B beads, $\rho(y)$, along Y axis. It can be evaluated within a thin cross-section slabs located in the middle of each region (marked as $1-4$ in the third frame from the left in Fig. 4). The thickness of each cross-section slab in X direction is equal to 2 and the averaging of the density is made in Z-direction. The histograms for the density profiles $\rho^{(i)}(y)$ in each i-th slab obtained in this way for the morphology shown in the third frame from the left in Fig. 4, are presented in the left frame of Fig. 5. The local density inside each column of B beads is equal to the bulk density, $\rho(y) \approx \rho = 3$, whereas outside the column it drops down to zero. Therefore, the integrated density, $I = \int_0^{L_y} dy\rho(y)/L_y$ is a good measure for "block continuity". Right frame of Fig. 5 shows the values of I, averaged over all four slabs, $1-4$. Two sets of simulations were performed. For the set I we started the simulation from the morphology equilibrated at $f_B = 0.5$ and converted required number of B beads, chosen randomly across the system, into A beads. In the set II simulation, the initial configuration involved linearly stretched polymer chains and solvent A and B beads randomly distributed within the pore.

One can observe the transformation from continuous into disconti-

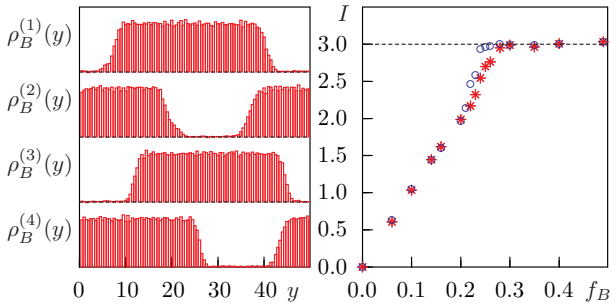

Figure 5. Left frame shows the density profiles $\rho^{(i)}(y)$ along each i-th slab region shown in the third frame from the left in Fig. 4. Right frame shows the dependence of the integral profile I (averaged over four slabs) on f_B. The results for simulation set I are shown as blue disks and for the set II – as red asterisks.

nuous block morphology that occurs at $f_B^* \approx 0.23$ (for the simulations set I; blue open disks) or at $f_B^* \approx 0.28$ (for the simulation set II; red asterisks). The former value is lower indicating the presence of the "underconcentrated" continuous block morphology at $0.28 > f_B > 0.23$ in the simulations set I. It is also interesting to note that for small f_B the integral I changes nearly linearly with f_B.

4. Competition between solvent mediated morphologies for closely arranged stripes

So far we considered several special cases when both the geometry restrictions imposed by the pore geometry and the composition of the mixture confined within accessible sub-regions promote essential morphological changes. In both cases of a narrow pore (subsection 3.2) and of a pillar (subsection 3.3) the stripes of brushes are bridged in one of directions by purely geometry means, literally by bringing stripes close enough to form lamellae (pillars). The role of the solvent is restricted then to swelling of already formed lamellae (pillars) and to micro-phase separation inside the polymer-free sub-regions.

However, one can envisage the situation when the lamellar (pillar) bridges are formed exclusively due to the role of a solvent. This, obviously, is possible in the geometries where the stripes of brush are brought sufficiently close in one of X or Z dimensions, but not close enough to bridge over by theirselves. Even more promising case can be designed by

provoking the competition between bridging, which may happen when the stripes are positioned sufficiently close in both X and Z directions. Possible technological applications could involve the use of a solvent mixture which contains A component in a form of a short chain. This component could be used first for demixing with B component and formation of certain morphology, and then to be used as a crosslinker, to fix the structure permanently.

4.1. Mechanism for solvent-medialted morphologies and quantitative characterization of brush bridging and chains deformation

The mechanism for the solvent-mediated morphologies lies in swelling of a polymer brush due to adsorption of a good solvent, the effect already mentioned above. Here we will discuss this effect in more detail. Let us consider the environment within the stripes of polymer chains. Due to relatively low grafting density $\rho_g = \frac{1}{3}\rho$ (where $\rho = 3$ is bulk number density) the stripes are far from the regime of a dense brush [34] and are exposed to available solvent. For the case of poor solvent the brush collapses and each chain found itself is in a regime of polymer melt, whereas for a good solvent the chains are expected to be in the regime of a good solution. Two cases are well distinguished by their respective scaling laws, [35]. For instance, the radius of gyration scales as:

$$R_g = R(l_0(N-1))^{\nu} \tag{1}$$

where $R = \text{const.}$, l_0 is the equilibrium bond length, N is the number of monomers and $\nu = 0.5$ for the case of polymer melt and $\nu \approx 0.59$ (Flory exponent) for the case of a good solution. [35] As it was discussed previously, [36] the softness of the potentials employed in typical DPD simulations does not violate the correct value for the exponent $\nu = 0.59$ for a single chain in a good solvent.

To check whether this scenario holds, we performed a set of simulations for the pore geometry with well separated stripes. Polymer chains are made of A beads and one-component solvent of C beads is used. The quality of the solvent is tuned via the repulsion parameter a_{AC} between A and C beads ranging from 25 (good solvent) up to 40 (bad solvent). For each simulation run, the average bond length l_0 and radius of gyration R_g were evaluated and the scaling law (1) was employed for the assumed values of the exponent ν, $\nu = 0.5$ or 0.59. Next, the prefactor R (see Eq. (1) was estimated. The results are collected in Table 4.1. As it follows from the enclosed data, the difference between the estimated

prefactors R does not exceed 1% which proves that the scaling law (1) holds consistently. These simulations confirm a crossover from the regime of polymer melt to a good solution regime for each chain which is driven by the quality of the solvent. Typical chain extension ratio is estimated as $(l_0(N-1))^{0.09} \sim 1.3$ which is of the order of $2-4$ unit lengths for our particular model and this provides the lengthscale for brush separations at which one expects solvent-mediated bridging.

pore geometry	solvent	l_0	R_g	R
$d = 22$, in-phase	$a_{AC} = 40$ ($\nu = 0.50$)	0.893	1.909	0.463
	$a_{AC} = 25$ ($\nu = 0.59$)	0.937	2.557	0.468
$d = 20$, out-of-phase	$a_{AC} = 40$ ($\nu = 0.50$)	0.892	1.909	0.464
	$a_{AC} = 25$ ($\nu = 0.59$)	0.936	2.558	0.468

Table 1. Results of fitting the average bond length l_0 and radius of gyration R_g to the scaling law, Eq. 1 for the assumed values of the exponent ν. Output: prefactor R in Eq. 1 is numerically consistent for all the considered cases.

To characterize quantitatively the level of bridging between stripes we introduce the overlap integrals I_x and I_z between polymer chains in X and Z directions (in analogy to the case of uniform brushes [37]):

$$I_x = \sum_{\langle ik \rangle} \int_0^{L_x} \rho_i(x)\rho_k(x)dx \cdot \left[\sum_{\langle ik \rangle} \int_0^{L_x} dx \right]^{-1}, \qquad (2)$$

$$I_z = \int_0^{d} \rho_{\rm bot}(z)\rho_{\rm top}(z)dz \cdot \left[\int_0^{d} dz \right]^{-1},$$

where $\rho_i(x)$ is the density profile along X axis for polymer beads belonging to i-th stripe (averaged over Y and Z directions); $\rho_{\rm bot}(z)$ and $\rho_{\rm top}(z)$ are density profiles for polymer beads belonging to bottom or top wall, respectively (averaged over X and Y directions). These density profiles are illustrated in Fig. 6. The evaluation of I_x overlap integral is performed over all $\langle ik \rangle$ pairs that are located at the same wall and are adjacent in X direction (with the account of the periodic boundary conditions).

Bridging of brushes involves certain amount of bending and/or anisotropic stretching of polymer chains, these can be quantified via the components of gyration tensor, G_{xx}, G_{yy} and G_{zz}. The components are

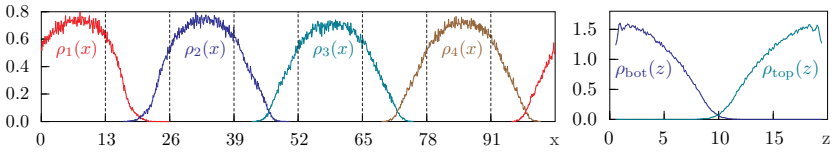

Figure 6. Left frame illustrates density distributions $\rho_i(x)$ of the polymer beads in each i-th stripe along X axis averaged over Y and Z axes (the distributions $1-4$ belonging to the bottom surface are shown only). Right frame illustrates density distributions of the polymer beads along Z axis that belong to bottom and top surfaces (abbreviated as "bot" and "top" respectively), the distributions are averaged in X and Y directions.

evaluated for each k-th chain

$$G^{[k]}_{\alpha\beta} = \frac{1}{N}\sum_{i=1}^{N}(r^{[k]}_{i,\alpha} - R^{[k]}_{\alpha})(r^{[k]}_{i,\beta} - R^{[k]}_{\beta}), \qquad (3)$$

where α, β denote Cartesian axes, $r^{[k]}_{i,\beta}$ are the positions of individual monomers and $\mathbf{R}^{[k]}$ is the center of mass position of the k-th chain. Then, $G^{[k]}_{\alpha\beta}$ are averaged over chains and over time trajectory after the morphology stabilizes itself, providing the estimates for G_{xx}, G_{yy} and G_{zz}. One should mention that due to the symmetry of the pore in Y direction, the G_{yy} component is found to be unchanged and it is not considered in our analysis. The average radius of gyration R_g is defined as $R_g^2 = G_{xx} + G_{yy} + G_{zz}$, and the average extension of chains can be found from the maximal eigenvalue of the gyration tensor, $\sigma^2_{\rm max}$.

4.2. Solvent-mediated morphological changes

The properties introduced above are used to characterize solvent-mediated bridging between stripes of brushes. At first we will consider the case of one-component solvent of variable quality (tuned via a_{AC} parameter, see above). The results are provided for the pore size of $d = 20$ and stripes od width $w = 13$ arranged out-of-phase (see Fig.7). With a decrease of a_{AC} towards the case of a good solvent ($a_{AC} = 25$), one observes a monotoneous increase of all the metric properties, G_{xx}, G_{zz} and $\sigma^2_{\rm max}$. This quantifies the effect of polymer chains swelling due to the crossover from the polymer melt to polymer in a good solvent regime. The overlap integrals I_x and I_z have been found to become non-zero at certain threshold value of $a_{AC} < 28$. This indicates solvent-mediated

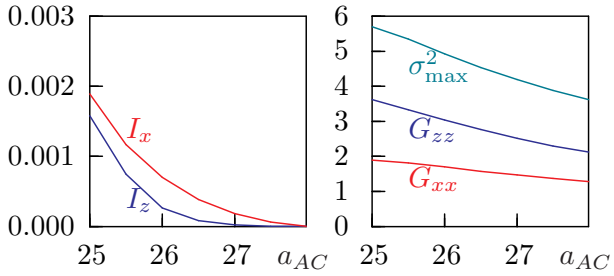

Figure 7. Behavior of the overlap integrals I_x and I_z (left frame) and the components G_{xx} and G_{zz} and maximal eigenvalue $\sigma^2_{\max}$ of the gyration tensor (right frame) upon the changes of the quality of the one-component solvent. The quality of the solvent is defined via repulsion parameter a_{AC} between polymer (A) and solvent (C) beads, the value of $a_{AC} = 25$ represents the case of a good solvent.

bridging between droplets of polymer chains. The bridging happens almost simultaneously in both X and Z directions for this geometry of the pore. In the view of our analysis, it is important to mention that all the characteristics, I_x, I_z, G_{xx}, G_{zz} and $\sigma^2_{\max}$ increase monotonically with a decrease of a_{AC} down to 25 with no peculiarities observed neither in the behavior of metric properties and overlap integrals nor in the snapshots.

The case of one-component solvent of variable quality provides a suitable reference point for a more complex case of a two-component solvent composed of A and B beads. The repulsion parameter a_{AB} is chosen to be always equal to 40 in our study, therefore, the effective "goodness" of such a mixture can be characterized by the fraction f_B of B beads (the mixture is a good solvent for $f_B = 0$). The analogy with one-component solvent is, however, not exact, as far as the mixture is prone to segregation (see, e.g. Fig. 4 in Ref. [30]). Local inhomogeneities may influence the way in which the brushes are bridged and, as the result, the sequence of solvent-mediated morphologies may differ from the case of one-component solvent. Hereafter we will consider fixed stripe width of $w = 13$ and both: in- and out-of phase arrangements. The pore size will be fine-tuned in each case and ranges from $d = 19$ to $d = 24$.

In the case of in-phase arrangement of the stripes we select three pore sizes, namely $d = 20, 22$ and 24 (the distance between brushes in X and Z directions is approximately equal for $d = 22$). The evolution of I_x, I_z, G_{xx}, G_{zz} and $\sigma^2_{\max}$ upon the change of the fraction of f_B from 0.5 down

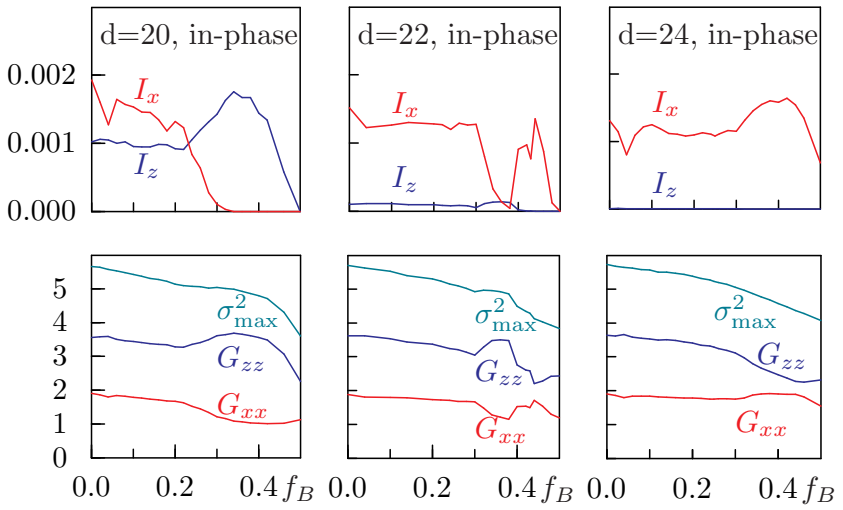

Figure 8. Behavior of the overlap integrals I_x and I_z (top row of frames) and the components G_{xx} and G_{zz} and the maximal eigenvalue $\sigma^2_{\max}$ of the gyration tensor (bottom row of frames) upon the changes of the effective quality of the two-component solvent of A and B beads. Effective quality of the solvent is defined via the fraction f_B of "bad solvent" beads B. The case of in-phase arrangement of stripes of the width $w = 13$ is shown at the pore sizes $d = 20, 22$ and 24.

to 0 is shown for each pore size in Fig. 8. One can compare these plots with the curves displayed in Fig. 7 and observe that the metric properties of chains at $f = 0.5$ subject to the two-component solvent match approximately their counterparts for the case of one-component solvent at $a_{AC} = 28$. This provides the estimate for an effective "goodness" of the two-component solvent. Metric properties coincide for the case of good solvent ($f = 0$ and $a_{AC} = 25$, respectively).

When one moves away from $f_B = 0.5$ towards 0 the behavior of all the properties I_x, I_z, G_{xx}, G_{zz} and $\sigma^2_{\max}$ differs much from the case of one-component solvent. For the pore of $d = 20$, the bridging in Z direction is observed first. This is indicated by a large hill at I_z centered around the value of $f_B = 0.34$ (top left frame in Fig. 8). To be able to form the pillar morphology, the chains need to rearrange their selves preferentially in Z direction as indicated by an increase of G_{zz} at the expense of G_{xx} values (bottom left frame in Fig. 8). The value of $G_{zz} = 3.69$ found at $f_B = 0.34$ is of same order and even exceeds that observed at $f_B = 0$,

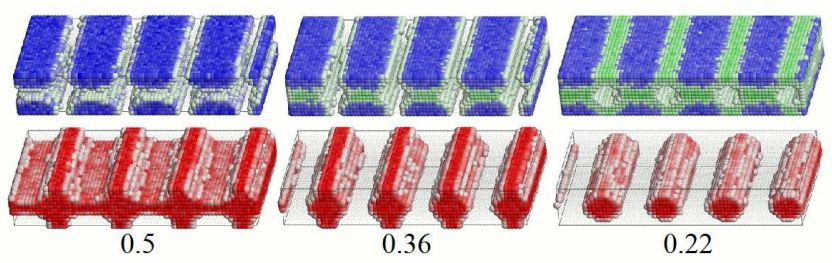

Figure 9. Sequence of morphologies obtained for $d = 20$ and for in-phase arranged stripes of the width $w = 13$ at various fractions f_B (indicated at the bottom). Top row: color-coded densities of brush prevailing (blue) and good solvent prevailing (green) regions, bottom row: bad solvent prevailing regions (red). Morphologies: separate droplets ($f_B = 0.50$); solvent mediated pillars ($f_B = 0.36$) and in-lined cylinders of B beads ($f_B = 0.22$).

namely $G_{zz} = 3.56$. This indicates that the chains within pillars are in the regime of a good solvent. This is confirmed by the snapshots shown in top-middle and bottom-middle columns of Fig. 9, where the droplets are seen merged together by the good solvent beads. Therefore, as the result of different miscibility of A and B components, the solvent A nucleates by filling the gap between polymer droplets, and solvent mediated transition from separate droplets to pillar morphology occurs. With further decrease of f_B, the pillars are also bridged in X direction. This is indicated by an increase of G_{xx} values and is seen in the top-right and bottom-right columns of Fig. 9.

With an increase of the pore size d to 22, the bridging ability in Z direction is lessened giving a way for bridging along the walls. This is demonstrated by the existence of local maxima and minima of I_x, I_z and G_{xx} and G_{zz} components (see top-center and bottom-center frames in Fig. 8). With further increase of d to 24 the situation is reversed with respect to the case of $d = 20$. Now, the droplets are farer in Z direction and their bridging is observed in X direction: I_x and G_{xx} posses maxima centered around $f_B = 0.4$ (top-right and bottom-right frames of Fig. 8).

Let us switch now to the case of out-of-phase arrangement of stripes. The set of pore sizes $d = 19, 20$ and $d = 21$ are analyzed in this case (the distance between brushes in X and Z directions is approximately equal for $d = 20$). The behavior of I_x, I_z, G_{xx}, G_{zz} and $\sigma^2_{\max}$ is shown in Fig. 10. The limiting cases of $d = 19$ and $d = 21$ bear similarities

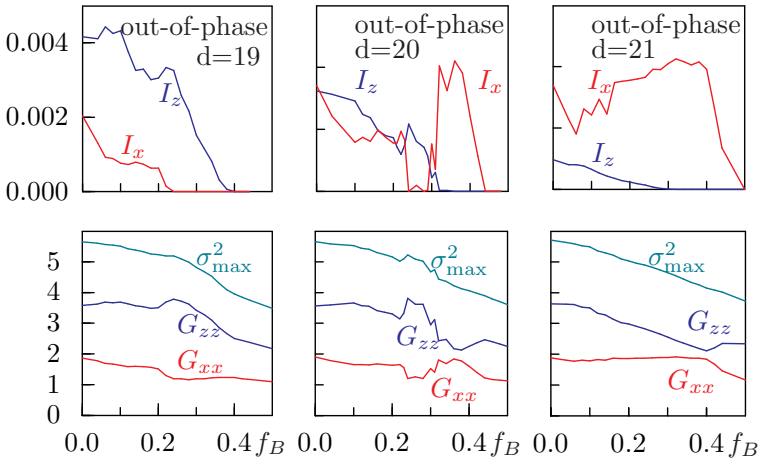

Figure 10. The same properties as in Fig. 8 are shown for the case of out-of-phase arrangement of stripes of the width $w = 13$ at the pore sizes $d = 19, 20$ and 21.

to their respective counterparts ($d = 20$ and $d = 24$) for the in-phase arrangement of stripes. Indeed, at $d = 19$ the polymer-rich droplets are bridged in Z direction first with a decrease of f_B. With further decrease of f_B the droplets are bridged in X direction. Situation is reversed at $d = 21$.

The intermediate case of the pore size $d = 20$ is more interesting because it demonstrates solvent mediated switching between various morphologies. When f_B decreases away from 0.5, first the bridges in X direction are formed. Both I_x and G_{xx} exhibit maxima centered around $f_B = 0.36$, cf. top-middle and bottom-middle frames of Fig. 10. This indicates the formation of solvent mediated lamellar morphology, see snapshots in top-middle and bottom middle frames of Fig. 11. With further decrease of f_B, the bridges are formed in Z direction at the expense of those that have been previously formed in X direction. This is indicated by large value of I_z and practically zero value of I_x within the interval of $f_B \in [0.23, 0.3]$. The structure of this morphology is of simple meander (see snapshots in top-right and bottom-roght frames of Fig. 11).

One can see that upon increase of the fraction of good solvent in the system, the chains within each stripe swell and acquire certain bistability properties. The chains can redistribute their mass either in X or in Z direction (as indicated by the behavior of G_{xx} and G_{zz} components)

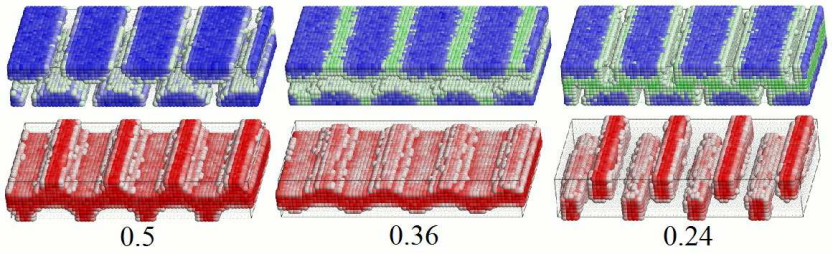

Figure 11. Sequence of morphologies obtained for $d = 20$, for out-of-phase arranged stripes of the width of $w = 13$ at various fractions of f_B. Separate droplets ($f_B = 0.50$); modulated lamellar ($f_B = 0.36$) and meander ($f_B = 0.24$) morphologies.

and form relevant bridges (as indicated by non-zero values of the overlap integrals I_x and I_z). The histograms for the corresponding components of the gyration tensor, $f(G_{xx})$ and $f(G_{zz})$ provide additional insight into spatial redistribution of the polymer chains in various morphologies. These histograms are shown in Fig. 12 for the case of pore size $d = 20$ and out-of-phase arrangement of the stripes of the width of $w = 13$.

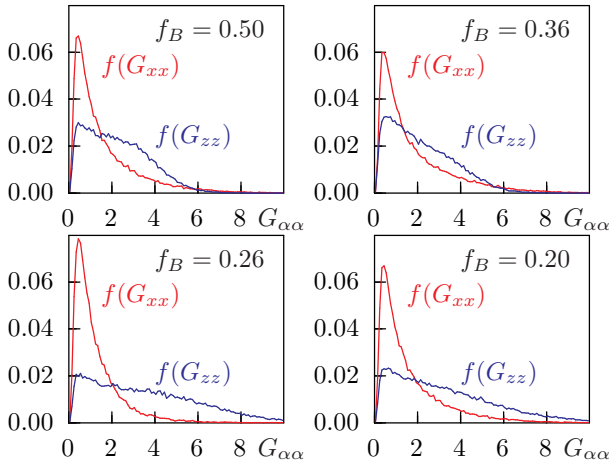

Figure 12. Distributions of the relevant gyration tensor components, G_{xx} and G_{zz} for the various fractions f_B (indicated in each frame). The case of $d = 20$, $w = 13$ and out-of-phase arrangement of stripes is shown.

The distribution function $f(G_{zz})$ is found to be essentially stretched towards larger values of G_{zz} for meander ($f_B = 0.26$) morphology and at still lower values of f_B. It exhibits a quite irregular shape, whereas the distribution of $f(G_{xx})$ is similar to the Lhuillier form [36, 38, 39] that was found as a typical distribution of experimental radii of gyration for long polymers. Broad distributions of the gyration tensor of both components indicate the existence of weakly and highly deformed chains within each stripe. It is plausible to assume that highly deformed chains are found within the bridges that connect polymer droplets in solvent mediated pillar, meander and possibly other morphologies. A measure for the average stretch of chains is provided by the maximal eigenvalue of the gyration tensor, $\sigma^2_{\max}$. As it follows from the set of plots shown in Figs. 8 and 10, the values of $\sigma^2_{\max}$ exhibit local maxima for certain morphologies. The values of these maxima are higher as compared to the case of one-component solvent mapped into an effective value of a_{AC} (see Fig. 7). This indicates that the loss of conformation entropy due to excess average stretch of chains is compensated by an decrease of the enthalpy, due to an increase of contacts between similar beads of type A.

5. Summary

In this work we consider formation and transitions between the nanostructures that occur inside a pore modified by stripes of tethered polymer brushes filled by a binary mixture. The beads A of filler solvent are identical to these of chain monomers, while the beads B exhibit partial mixing with beads A. Two options of in- and out-of-phase arrangement of polymer stripes are considered for a broad range of pore geometies and at various composition of A and B beads. For some cases we also undertook supplementary simulations with the one-component solvent of variable quality which replaces the mixture, to serve as a reference.

The change of the composition of the fluid inside the pores has a great impact on the developing structures. For pore geometries with narrow stripes the problem of the description of microphase separation inside the pore reduces to quasi two-dimensional; in the case of moderately wide stripes and narrow pore one faces quasi one-dimensional demixing; whereas for very wide stripes the system is split into quasi two-dimensional and bulk regions.

The most interesting, in our view, effects that demonstrate solvent mediated changes in the nanostructures occur for the geometries with weakly separated stripes of polymer chains. With the increase of A component, the latter dissolves the polymer chains causing their swelling.

As the result of this, the system acquires a bistability in terms of either bridging adjacent stripes along the wall or bridging opposite stripes across the pore. Stable morphology is formed as the result of a competition between seggregation of A and B beads and the deformation of the chains. In our simulations we observe morphology switching due to subtle changes in pore geometry and/or the composition of a mixture.

We found following solvent mediated morphologies: in-lined cylinders (made of one component), meander structure and wave-shaped modulated internal channels. Suggested applications of such structures (after, possibly, making the structure permanent via crosslinking) involve nanopatterning for manufacturing of nanochannels, nanorods and similarly sized objects.

So far our studies concentrated on the equilibrium DPD simulations. However, it would be of interest to check how the morphologies change if the fluid would undergo a pressure-driven flow along the pore axis. The last problem is currently under study in our laboratories.

Acknowledgments

This work was supported by EC under the Grant No. PIRSES 268498. J.I. is thankful to T. Kreer, S. Santer and D. Neher for fruitful and stimulating discussions.

References

1. P. G. de Gennes, Rev. Mod. Phys. **57**, 827 (1985).
2. R. C. Advincula, W. J. Brittain, K. C. Caster and J Ruhe, *Polymer Brushes: Synthesis, Characterization, Applications*, Willey, New York (2004).
3. J. Rühe, M. Ballauf, M. Biesalski, P. Dziezok, F. Grohn, D. Johannsmann, N. Houbenov, N. Hugenberg, R. Konradi, S. Minko, M. Motornov, R. R. Netz, M. Schmidt, C. Seidel, M. Stamm, T. Stephan, D. Usov and H. N. Zhang, Adv. Polym. Sci. **165**, 79 (2004).
4. A. Naji, C. Seidel and R. R. Netz, Adv. Polym. Sci. **198**, 149 (2006).
5. L. I. Klushin and A. M. Skvortsov, J. Phys. A: Math. Theor. **44**, 473001 (2011).
6. K. Binder, T. Kreerb and A. Milchev, Soft Matter, **7**, 7159 (2011).
7. R. C. Advincula, W. J. Brittain, K. C. Caster, and J. Rühe (ed.) *Polymer Brushes*, Wiley-VCH, Weinheim, 2004.
8. R. Descas, J.-U. Sommer and A. Blumen, Macromol. Theory Simul., **17**, 429 (2008).

9. F. Garbassi, M. Morra and E. Occhiello, *Polymer surfaces: from physics to technology*, John Wiley & Sons; New York 2002.
10. L. H. Sperling, *Polymeric multicomponent materials: an introduction LED*. Wiley Interscience, New York 1997.
11. J. Klein, Science **323**, 47 (2009).
12. D. H. Napper, *Polymeric Stabilization of Colloidal Dispersions*, Academic, London 1983.
13. G. Storm, S. O. Belliot, T. Daemen and D. D. Lasic, Adv. Drug Delivery Rev., **17**, 31 (1995).
14. A. Hucknall, S. Rangarajan and A. Chilkoti, Adv. MAterials **21**, 2441 (2009).
15. A. J. Wang, J. J. Xu and H. Y. Chen, J. Chromatogr. A **120**, 1147 (2007).
16. Y. Li, J. Zhang, L. Fang, T. Wang, S. Zhu, Y. Li, Z. Wang, L. Zhang, L. Cui and B. Yang, Small **7**, 2769 (2011).
17. O. A. Guskova and C. Seidel, Macromolecules **44**, 671 (2011).
18. J. Wang and M. Müller, Macromolecules **42** , 2251 (2009).
19. Y. Yin, P. Sun, B. Li, T. Chen, Q. Jin, D. Ding and A.-C. Shi, Macromolecules **40**, 5161 (2007).
20. E. Bormashenko, R. Pogreb, O. Stanevsky, Y. Bormashenko, S. Tamir, R. Cohen, M. Nunberg, V. Z. Gaisin, M. Gorelik and O. V. Gendelman, Mater. Lett. **59**, 2461 (2005).
21. U. Nagpal, H. Kang, G. S. W. Craig, P. F. Nealey and J. J. de Pablo, ACS Nano, **5**, 5673 (2011).
22. Q. Cao, C. Zuo, L. Li, Y. Yang and N. Li, Microfluid Nanofluid **10**, 977 (2011).
23. T. Chen, I. Amin and R. Jordan, Chem. Soc. Rev. **41**, 3280-3296 (2012)
24. L. Guangsuo, *Fabrication of nanopatterns via surface chemical modification and reactive reversal nanoimprint lithography*, PhD Thesis, National university of Singapore, Singapore 2010, http://scholarbank.nus.edu.sg/handle/10635/22850
25. D. W. L. Tolfree, Rep. Prog. Phys. **61**, 313 (1998); F. Burmeister, C. Schläfle, B. Keilhofer, C. Bechinger, J. Boneberg and P. Leiderer, Adv. Mater. **10**, 495 (1998); J. B. Knight, A. Vishwanath, J. P. Brody and R. H. Austin, Phys. Rev. Lett. **80**, 3863 (1998).
26. *Surface-Initiated Polymerization I and II.* (Ed. : R. Jordan), in Advances in Polymer Science, **197/198**, Springer, Berlin, (2006); X. Zhou, Y. Chen, B. Li, G. Lu, F. Y. C. Boey, J. Ma and H. Zhang, Small **4**, 1324 (2008); U. Schmelmer, A. Paul, A. Küller, M. Steenackers, A. Ulman, M. Grunze, A. Gölzhäuser and R. Jordan,

Small **3**, 459 (2007).
27. P. Adamczyk, P. Romiszowski and A. Sikorski, Catal. Lett. **129**, 130 (2009); C.-Y.Chang, H.-W. Yang, J.-S. Lin, S.-P. Ju and J.-Y. Hsieh, J. Comput. Theor. Nanosci. **8**,2439 (2011); S. K. Singh, S. Khan, S. Jana and J. K. Singh, Molec. Simul. **37**, 350 (2011); A. G. Koutsioubas and A. G. Vanakaras, Langmuir **24**, 13717 (2008); H. Chen, X. Chen, Z. Ye, H. Liu and Y. Hu, Langmuir **26**, 6663 (2010).
28. A. Jayaraman, C. K. Hall and J. Genzer, J. Chem. Phys. **123**, 124702 (2005); ; H. Chen, C. Peng, L. Sun, H. Liu, Y. Hu and J. Jiang, Langmuir **23**, 11112 (2007)
29. J. R. Spaeth, T. Dale, I. G. Kevrekidis and A. Z. Panagiotopoulos, Ind. Eng. Chem. Res. **50**, 69 (2011); M. Patra and P. Linse, Nano Lett. **6**, 133 (2006). F. Goujon, P. Malfreyt and D. J. Tildesley, J. Chem. Phys. **129**, 034902 (2008). C.-S. Li, W.-C. Wu, Y.-J. Sheng and W.-C. Chen, J. Chem. Phys. **128**, 154908 (2008); P. Petrus, Martin Lísal and J. K. Brennan, Langmuir **26** 3695; 14680 (2010).
30. J.M. Ilnytskyi, T. Patsahan, S. Sokołowski, J. Chem. Phys. **134**, 204903 (2011).
31. R.D. Groot and P.B. Warren, J. Chem. Phys. **107**, 4423 (1997).
32. J. M. Ilnytskyi, T. Patsahan, M. Holovko, P. E. Krouskop, and M. P. Makowski, Macromolecules **41**, 9904 (2008).
33. Y. Zhao, H. Liu, Zh. Lu, and Ch. Sun, Chin. J. Chem. Phys. 21, 451 (2008).
34. D. Romeis, H. Merlitz, J.U. Sommer, J. Chem. Phys. **136**, 044903 (2012).
35. P.G. de Gennes. Scaling Concepts in Polymer Physics. Cornell University Press, Ithaca and London, 1979.
36. J.M. Ilnytskyi, Yu. Holovatch, Condens. Matter Phys. **10**, 539 (2007).
37. T. Kreer, M.H. Müser, K. Binder, and J. Klein, Langmuir **17**, 7804 (2001).
38. D. Lhuillier, J. Phys. France **49**, 705 (1988).
39. J.M. Victor, D. Lhuillier, J. Chem. Phys. **92**, 1362 (1990).

CONDENSED MATTER PHYSICS

The journal **Condensed Matter Physics** is founded in 1993 and published by Institute for Condensed Matter Physics of the National Academy of Sciences of Ukraine.

AIMS AND SCOPE: The journal **Condensed Matter Physics** contains research and review articles in the field of statistical mechanics and condensed matter theory. The main attention is paid to physics of solid, liquid and amorphous systems, phase equilibria and phase transitions, thermal, structural, electric, magnetic and optical properties of condensed matter. Condensed Matter Physics is published quarterly.

ABSTRACTED/INDEXED IN: Chemical Abstract Service, Current Contents/Physical, Chemical&Earth Sciences; ISI Science Citation Index-Expanded, ISI Alerting Services; INSPEC; "Referatyvnyj Zhurnal"; "Dzherelo".

CONTACT INFORMATION:
Institute for Condensed Matter Physics
of the National Academy of Sciences of Ukraine
1 Svientsitskii Str., 79011 Lviv, Ukraine
Tel: +38(032)2761978; Fax: +38(032)2761158
E-mail: cmp@icmp.lviv.ua http://www.icmp.lviv.ua